

# Feedback Control of HVOF Thermal Spray Process Accounting for Powder Size Distribution

Mingheng Li and Panagiotis D. Christofides

(Submitted 13 February 2002; in revised form 19 August 2002)

This work presents a novel formulation of the control problem and a feedback control system for the high velocity oxygen-fuel (HVOF) thermal spray process, which explicitly accounts for the effect of powder size distribution. Initially, based on model predictions and available experimental data, the control problem is formulated as one of regulating appropriate averages (with respect to the particle volume distribution) of the temperature and velocity of the particles at the point of impact on substrate (these are the variables that directly influence coating microstructure and porosity, which, in turn, determine coating mechanical and thermal properties) by manipulating the oxygen/fuel ratio and the combustion chamber pressure, respectively. Then, a feedback control system is developed and applied to a detailed mathematical model of the process. Closed-loop simulations show that the average particle velocity and temperature at the point of impact on substrate reach the desired values in a short time, which validates the feasibility of real-time implementation of feedback control on HVOF thermal spray systems. It is also shown that the proposed formulation of the control problem (which accounts for the effect of powder size distribution) leads to a solution of the control problem that is superior (with respect to the achievement of the desired control objectives) to a solution that assumes a monodisperse powder size distribution. Finally, the proposed control problem formulation and the feedback control system are shown to be robust with respect to disturbances in spray distance and particle injection velocity, and variations in powder size distribution.

**Keywords** feedback control, HVOF thermal spray, powder size distribution, process modeling

## 1. Introduction

The high velocity oxygen-fuel (HVOF) thermal spray technology is widely used to deposit a large variety of metal and cermet coatings to modify the surface properties of a base material (substrate). Using the thermal energy produced by the combustion of fuel with oxygen to heat and propel the powder particles, the HVOF thermal spray provides a highly efficient way to modify the surface properties of a substrate to extend product life, increase performance, and reduce maintenance costs. Recently, there is an increasing interest in the HVOF thermal spray processing of nanostructured coatings, whose grain size is less than about 100 nm.<sup>[1]</sup> This interest has been motivated by several factors, including (1) the cost-effective production of high-quality nanosized powders, (2) the superior qualities of coatings made with the HVOF process,<sup>[2]</sup> and (3) the discovery that nanostructured coatings exhibit superior qualities over traditional counterparts (made of materials with micro-sized grains) in several aspects including hardness, strength, ductility and diffusivity (e.g., Ref. 1 and 3).

Over the last decade, the need to optimally design and operate thermal spray processes has motivated significant research

on the development of fundamental mathematical models to capture the various physicochemical phenomena taking place in thermal spray processes and to describe the dynamic behavior of various process components. Specifically, fundamental models have been developed describing the gas dynamics and particle in-flight behavior inside of the gun and in the free jet<sup>[4-6]</sup>; molten droplet deposition, solidification and microstructure development<sup>[7]</sup>; and the relationship between coating microstructure and mechanical properties.<sup>[8]</sup> In addition, research has been carried out in the integration of the detailed models of the aforementioned components to develop general simulators that describe the behavior of entire thermal spray processes.<sup>[9]</sup>

To reduce product variability and to improve robustness with respect to variations in the operating conditions in industrial HVOF thermal spray processes, it is important to implement excellent real-time process diagnosis and control which could lead to the fabrication of coatings with microstructures that yield the desired properties. Despite the recent progress on the modeling of the various phenomena that affect droplet motion, deposition, solidification and microstructure development in HVOF spraying processes, at this stage, there exists no systematic framework for integrated on-line diagnosis and control of the HVOF thermal spray processing which will be capable of achieving precise regulation of the microstructure and ultimate mechanical and thermal properties of the sprayed coatings. In addition, incorporation of advanced real-time diagnosis and control schemes into thermal spray processes is expected to reduce operational cost and environmental impact, and allow depositing nanostructured and complex (multi-material) coatings with very low variability. Since the application of optimization and control techniques to

**Mingheng Li and Panagiotis D. Christofides**, Department of Chemical Engineering, University of California, Los Angeles, CA 90095-1592. Contact e-mail: pdc@seas.ucla.edu.

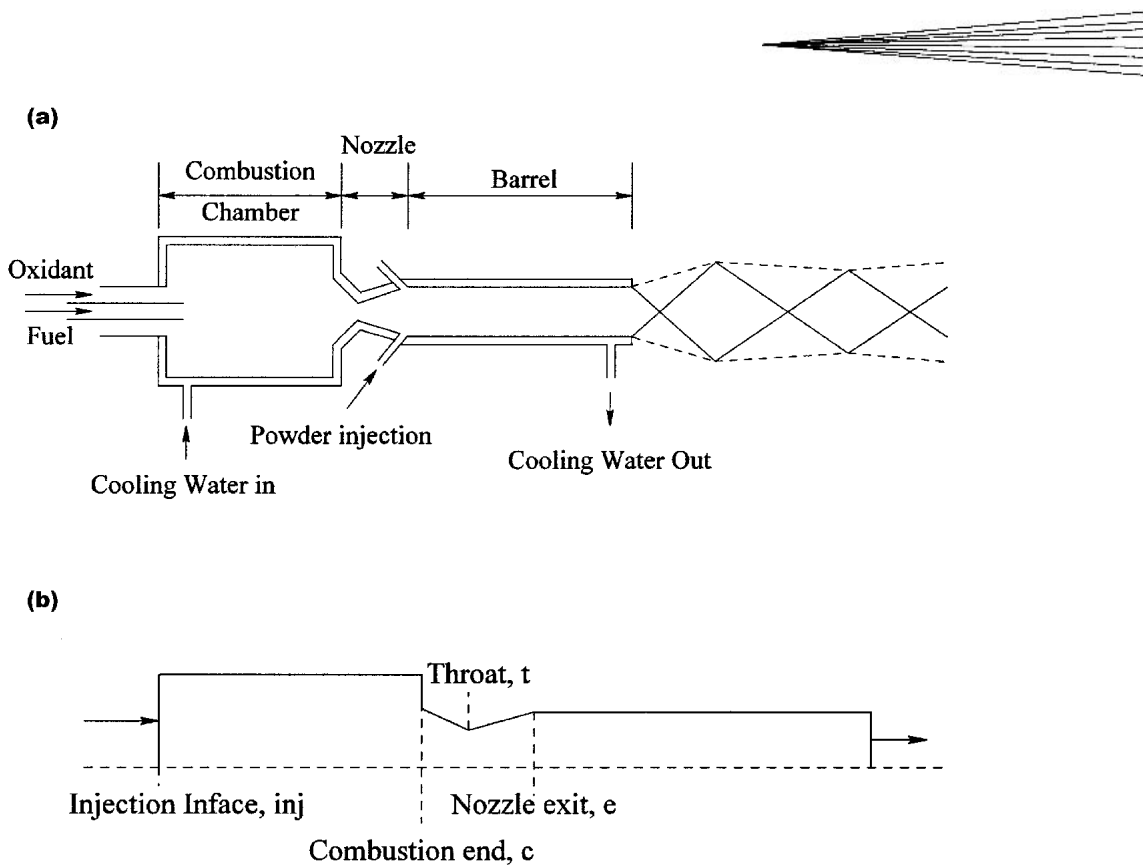


**Fig. 1** Schematic of the HVOF torch

spray casting processes has been reported to lead to significant improvements in their operation and performance (e.g., Ref. 10, 11), it is important to develop real-time computer control systems for thermal spray processes by integrating fundamental models that accurately describe the inherent relationships between the coating microstructure and the processing parameters with on-line state-of-the-art diagnostic techniques and control algorithms. Recent efforts in this direction have mainly focused on diagnostics and control of plasma thermal spray (see Ref. 12); the reader may also refer to Ref. 13 for a discussion of various process optimization and control issues.

This work presents a formulation of the control problem and a feedback control system for the HVOF thermal spray process, which explicitly account for the effect of powder size distribution. A fundamental model, which is computationally tractable while capable of capturing the dominant physicochemical phenomena occurring in the HVOF thermal spray process, is used to determine the controllable process variables that influence the temperature and velocity of particles at the point of impact on the substrate. These are two crucial parameters that directly affect coating microstructure and porosity, and eventually, coating strength, and hardness.<sup>[14]</sup> Based on the model predictions and available experimental data, the control problem is formulated as the one of regulating volume-based averages of the temperature and velocity of the particles at the point of impact on substrate by manipulating the oxygen/fuel ratio and the combustion chamber pressure, respectively. A feedback control system is then developed and applied to the HVOF process model. Extensive closed-loop simulations are performed to test the performance and robustness of the feedback control system and to

evaluate the effectiveness of the proposed control problem formulation.

## 2. Modeling of the HVOF Process

### 2.1 Process Description

Figure 1(a) shows the schematic diagram of a commonly used HVOF thermal spray system. It consists of a combustion chamber, a Laval nozzle (a duct of convergent-divergent area that produces supersonic flow) and a barrel. High pressure and high temperature combustion gases, which are generated by the reaction of fuel gases (typically propylene, propane, or hydrogen) and oxygen in the combustion chamber, are accelerated to supersonic velocity through the Laval nozzle. Using such a nozzle, gases can be significantly accelerated because a unique characteristic of compressible flow in the supersonic region is that increasing cross-sectional area of the channel results in increasing gas velocity.<sup>[15]</sup> Outside of the gun, the supersonic free jet adjusts to the ambient pressure by a series of compression and expansion waves, and visible shock diamonds are formed downstream of the barrel exit and are visible due to the associated temperature variations in the flame. The solid particles of metal or cermet powders are injected axially into the gas stream at the exit of the nozzle, where the pressure is not as high as that in the combustion chamber, so that powders can easily enter the gas stream. The powder particles are accelerated and heated in the barrel and in the free jet, and then impinge on the substrate with high velocity to make coatings.

Roughly speaking, there are three major processes involved

in the HVOF process: conversion of chemical energy into thermal energy by the combustion of fuel with oxygen in the chamber; partial conversion of thermal energy into kinetic energy of the burning gases by passing through the nozzle; and transfer of momentum and heat from gas to particles. To be able to develop a fundamental model for this process that is computationally tractable and can be used to determine the formulation of the control problem, it is assumed that the presence of particles has a negligible effect on the gas velocity and temperature field. This assumption is standard and reasonably accurate because the particle loading, which is defined as the ratio of mass flow rate of particles to that of gases, is typically less than 4%.<sup>[5]</sup> With this assumption, a one-dimensional model is used to simulate the internal and external gas flow/thermal field, and the particle trajectories and temperature histories are solved by momentum transfer and heat transfer equations. To further simplify the analysis, the following standard assumptions are also made: (1) the gas fluid dynamic/thermal field is at steady state; (2) the flame gas obeys the ideal gas law; (3) species reach equilibrium in the combustion chamber and the composition of the combustion products is frozen at the combustion condition along the Laval nozzle and barrel (this assumption was validated in Ref. 16 based on the comparison of experimental data and simulation results); (4) the combustion gases behave like a perfect gas during compression and expansion in the nozzle, and the ratio of specific heat at constant pressure to that at constant volume ( $c_p/c_v$ ) is nearly a constant; and (5) the friction and cooling water effects along the nozzle and barrel are negligible so that laws of isentropic flow (an ideal flow which is frictionless and adiabatic) of compressible fluids apply.

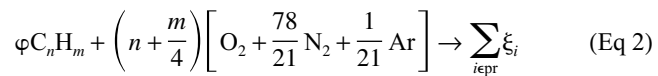
As shown in Fig. 1(b), the computational domain includes the combustion chamber, the Laval nozzle, and the barrel in the internal field and the supersonic free jet in the external field. The procedure that is followed for the numerical solution of the process model is the following: for a specified combustion chamber pressure and a fuel/oxygen ratio, the chemical composition and temperature in the combustion chamber, isentropic frozen flow along the Laval nozzle, frictionless flow along the barrel and the free jet outside of the gun are initially solved in sequence. Subsequently, the momentum transfer and heat transfer equations are incorporated in the gas dynamics to obtain the velocity and temperature profiles for each individual particle. Average particle velocity and temperature at the point of impact on substrate are calculated including the influence of the powder size distribution.

## 2.2 Modeling of Gas Flow and Thermal Fields

To calculate the equilibrium composition in the combustion chamber, the fuel/oxygen ratio needs to be specified first. In this work, the fuel/oxygen ratio is expressed by the equivalence ratio:

$$\varphi = \frac{F/O}{(F/O)_{st}} \quad (\text{Eq 1})$$

which is the actual fuel/oxygen ratio divided by the stoichiometric (denoted by the subscript st in the above equation) one. Based on this definition, the reaction of a hydrocarbon fuel and air can be represented by a general equation of the form:



where pr represents products and  $\xi$  is the molar fraction of component  $i$  in the combustion products. Given an equivalence ratio, the equilibrium composition and temperature in the combustion chamber can be calculated by minimizing the total Gibbs energy in the whole system subject to material and energy balances.<sup>[17]</sup> In this work, propane is used as the fuel gas and the oxidant is oxygen in the air stream. However, in several HVOF systems, for example, the Diamond Jet HVOF thermal spray developed by Sulzer Metco (Westbury, NY), pure oxygen is used as the oxidant, and air is used mainly as the coolant. When pure oxygen is used as the oxidant, the procedure followed to calculate temperature and composition of species in the chamber is similar; however, the equilibrium temperature and species composition using the same equivalence ratio will be different.

For isentropic compressible frozen flow along a Laval nozzle, the governing equations include continuity, momentum balance and energy balance. Based on these conservation equations, the ratio of gas properties (such as velocity, temperature, pressure, density) and cross-sectional areas at any two positions in the nozzle can be expressed as functions of the isentropic constant and the Mach number as follows<sup>[15]</sup>:

$$\frac{T_2}{T_1} = \frac{1 + [(\gamma - 1)/2]M_1^2}{1 + [(\gamma - 1)/2]M_2^2} \quad (\text{Eq 3})$$

$$\frac{P_2}{P_1} = \left\{ \frac{1 + [(\gamma - 1)/2]M_1^2}{1 + [(\gamma - 1)/2]M_2^2} \right\}^{\gamma/(\gamma-1)} \quad (\text{Eq 4})$$

$$\frac{\rho_2}{\rho_1} = \left\{ \frac{1 + [(\gamma - 1)/2]M_1^2}{1 + [(\gamma - 1)/2]M_2^2} \right\}^{1/(\gamma-1)} \quad (\text{Eq 5})$$

$$\frac{A_2}{A_1} = \frac{M_1}{M_2} \left\{ \frac{1 + [(\gamma - 1)/2]M_2^2}{1 + [(\gamma - 1)/2]M_1^2} \right\}^{(\gamma+1)/2(\gamma-1)} \quad (\text{Eq 6})$$

where  $T$ ,  $P$ , and  $\rho$  are the gas temperature, pressure, and density, respectively;  $A$  is the cross-sectional area perpendicular to the flow direction;  $\gamma$  is the isentropic constant defined as the heat capacity at constant pressure divided by that at constant volume; and  $M$  is the Mach number, or the ratio of gas velocity to the local sonic velocity

$$(a = \sqrt{\gamma P / \rho})$$

At the throat of the nozzle, where the gas flow field transits from subsonic flow to supersonic flow, the Mach number is 1. The reader may refer to Ref. 15 for a detailed derivation and discussion of Eq 3-6. The total mass flow rate, denoted by  $\dot{m}$ , is determined by

$$\dot{m} = A_t \left[ \gamma \rho_0 P_0 \left( \frac{2}{\gamma + 1} \right)^{(\gamma+1)/(\gamma-1)} \right]^{1/2} \quad (\text{Eq 7})$$

where  $A_t$  is the cross-sectional area at the throat, and  $\rho_0$  and  $P_0$  are the stagnation density and stagnation pressure, respectively. For the external flow and thermal fields, empirical formulae are used for the gas velocity and temperature decay,<sup>[18]</sup> which are



experimentally derived as functions of the distance from the exit of the HVOF gun.

### 2.3 Modeling of Particle Motion/Temperature

The particle trajectories and temperature histories in the gas field are computed by the momentum and heat transfer equations. Since the acceleration and deceleration of particles in the moving gas in the HVOF thermal spray system are dominated by the drag force,<sup>[19]</sup> the particle motion can be adequately described by the following two first-order ordinary differential equations:

$$m_p \frac{dv_p}{dt} = \frac{1}{2} C_D \rho_g A_p (v_g - v_p) |v_g - v_p|, v_p(0) = v_{p0} \quad (Eq\ 8)$$

$$\frac{dx_p}{dt} = v_p, x_p(0) = 0, \quad (Eq\ 9)$$

where  $m_p$  is the particle mass,  $v_p$  is the particle axial velocity,  $A_p$  is the projected area of the particle on the plane perpendicular to the flow direction,  $\rho_g$  is the gas density,  $C_D$  is the drag coefficient, and  $x_p$  is the particle position, calculated from the exit of the nozzle. Note that one difference between particle motion in a stagnant fluid and particle motion in a moving fluid is that there is an absolute sign in the relative velocity between particle and gas (term  $|v_g - v_p|$  at the right-hand side of the momentum equation) in the latter case, which guarantees that a particle is accelerated if its velocity is less than that of the gas and decelerated otherwise. To take into consideration the fact that many powders used in the HVOF process are not spherical, a formula for the drag coefficient  $C_D$ , which accounts for the particle shape using the concept of sphericity  $\psi$  (defined as the ratio of the surface area of a sphere with equivalent volume to the actual surface area of the particle), is used in this paper, which has the following form<sup>[20, 21]</sup>:

$$\frac{C_D}{K_2} = \frac{24}{Re K_1 K_2} [1 + 0.1118(Re K_1 K_2)^{0.6567}] + \frac{0.4305}{1 + 3305/Re K_1 K_2}, \quad (Eq\ 9)$$

where  $K_1$  and  $K_2$  are two sphericity-related factors. The local Reynolds number ( $Re$ ) for this two phase flow problem is defined based on the relative velocity  $Re = d_p/v_g - v_p/\rho_g/\eta_g$ , where  $d_p$  is either the particle diameter if the particle is spherical or the equivalent diameter if not, and  $\eta_g$  is the gas viscosity.

In the HVOF process, the Biot number of the particles ( $Bi = h/\lambda_p$ , where  $h$  is the heat transfer coefficient,  $x$  is a characteristic dimension defined by the ratio of particle volume to its surface area, and  $\lambda_p$  is the thermal conductivity of the particle) is typically less than 0.1<sup>[20]</sup>; this means that the particles are heated with negligible internal resistance, and temperature gradients inside them can be ignored.<sup>[22]</sup> Consequently, the equation describing the heat transfer between a single particle and the gas reduces to a first-order ordinary differential equation of the form:

**Table 1 Process Parameters Used in the Open-Loop Simulation**

Parameters	Values
Fuel	Propane
Oxidant	Air
Powder	Inconel 718
Barrel Diameter	1.0 cm
Barrel Length	0.2 m
Spray Distance	0.3 m
Ae/At	2.0
$\eta_g$	$5 \times 10^{-5}$ kg/m/s
$\lambda_g$	0.08 W/m/K
$\rho_p$	9000 kg/m <sup>3</sup>
$C_p$	462 J/kg/K
$\psi$	1.0

$$m_p C_p \frac{dT_p}{dt} = h A_p' (T_g - T_p), T_p(0) = T_0, \quad (Eq\ 10)$$

where  $T_p$  is the particle temperature,  $A_p'$  is the surface area of a particle, and  $h$  is the heat transfer coefficient computed by the Ranz-Marshall empirical equation<sup>[23]</sup>:

$$\frac{h d_p}{\lambda_g} = Nu = 2 + 0.6 Re^{1/2} Pr^{1/3}, \quad (Eq\ 11)$$

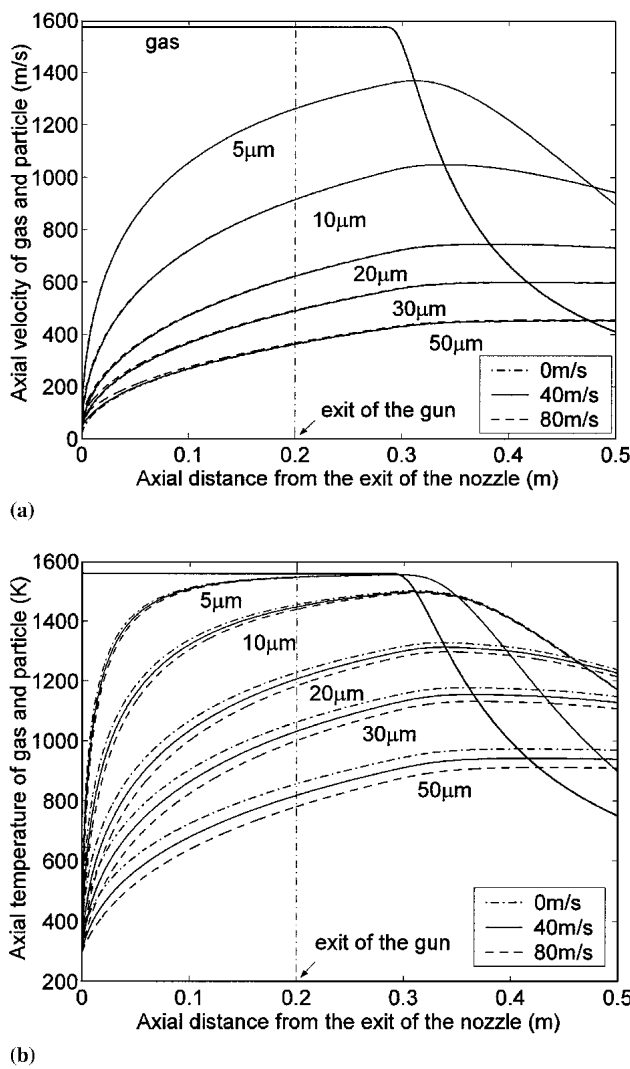
where the Prandtl number ( $Pr$ ) is calculated by  $Pr = C_p \eta_g / \lambda_g$ . We note that Eq 10 does not account for the effect of particle melting; such an effect is not considered in this work.

The equations for particle motion and temperature, together with the equation for gas temperature and velocity, are solved by numerical integration. Specifically, Eq 8 and 10 are integrated with a small enough time step ( $10^{-7}$  s) such that the gas velocity, gas temperature and local Reynolds number can be considered constant over the time interval of each time step. After one time step, the gas velocity and gas temperature are updated according to the new position of the particle and then the same strategy is repeated for the next step. This methodology was proposed in Ref. 24 and was shown to be computationally economical and accurate.

### 2.4 Process Model Simulation Results

Several simulation runs of the process model were performed to evaluate the effect of controllable process variables on particle velocity and temperature and to investigate the dependence of the particle velocity and temperature on particle size. The parameters used in these open-loop system (i.e., process model without feedback control) simulations are given in Table 1.

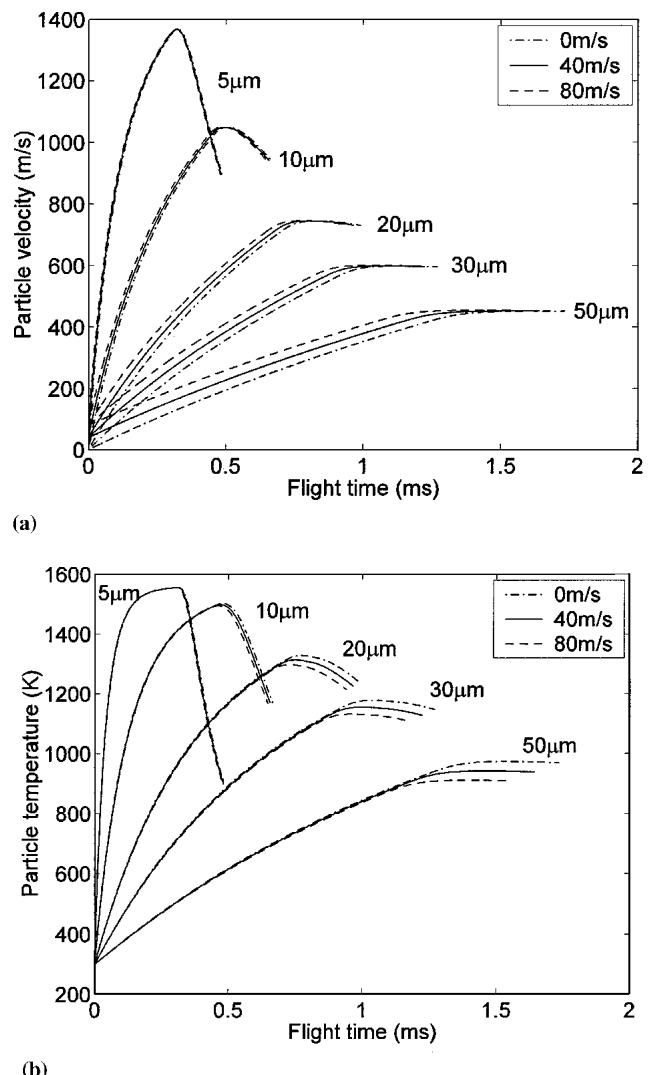
Figure 2 displays the axial velocity and temperature of gas and particles with different sizes along the flow field. To show the effect of particle injection velocity on the velocity and temperature profiles, the simulation was run under three different injection velocities (0, 40, and 80 m/s). Under each specific injection velocity, particles with different sizes are all accelerated in the barrel and in some region of the supersonic free jet (where their velocities are less than that of the combustion gases), and are decelerated after they reach the same velocity as that of the gas. Furthermore, fine particles change velocities more easily



**Fig. 2** (a) Axial velocity and (b) temperature profiles of gas and particle along the flow field for different particle sizes  $d_p = 5, 10, 20, 30$ , and  $50 \mu\text{m}$  under operating conditions  $p = 9 \text{ bar}$  and  $\varphi = 1.0$  and three different injection velocities  $v_{p0} = 0, 40$ , and  $80 \text{ m/s}$

than coarser ones due to their small momentum inertias. For example, a particle with a diameter of  $5 \mu\text{m}$  attains velocity as high as about  $1300 \text{ m/s}$  during flight. However, its velocity decreases rapidly. Particles with even smaller size fully track the motion of the exhaust gases and may not stick to the substrate. Similar behavior is also observed for the particle temperature. Note that in the processing of nanostructured coatings, it is of great significance to keep a relatively high particle temperature at the point of impact on the substrate while at the same time to prevent particles from being superheated during flight to reserve the nanocrystalline structure of particles. The behavior of particles with very small sizes in the gas stream explains why they are not suitable for thermal spraying.

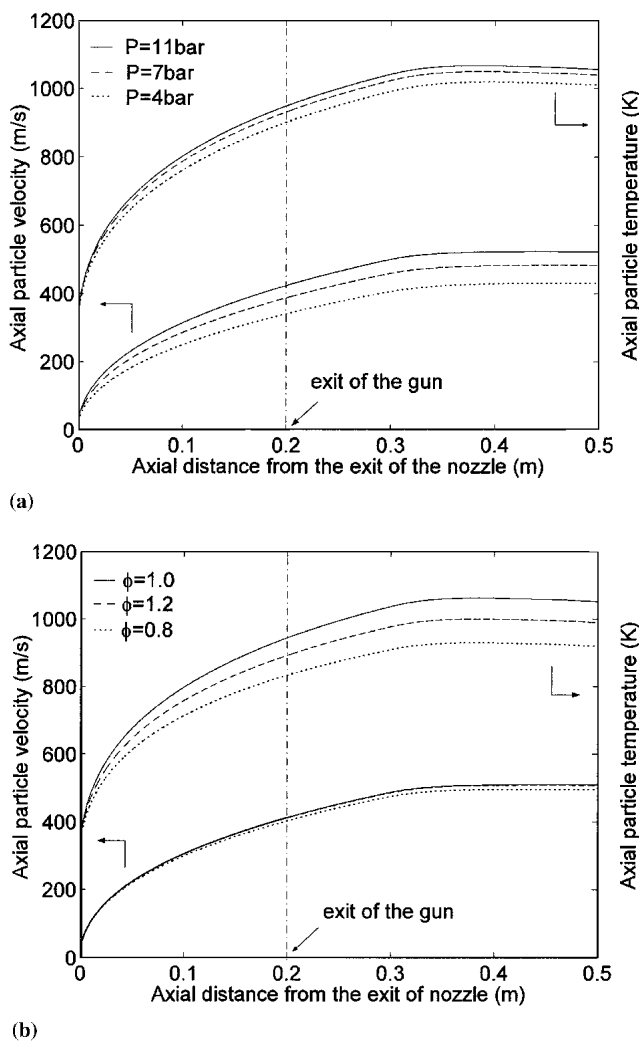
From the simulation runs of particle velocity and temperature along the gas field under three different particle injection velocities, we can conclude the following. First, the particle injection velocity has a minimal effect on particle velocity profile (except



**Fig. 3** (a) Axial velocity and (b) temperature as a function of flight time for different particle sizes  $d_p = 5, 10, 20, 30$ , and  $50 \mu\text{m}$  under operating conditions  $p = 9 \text{ bar}$  and  $\varphi = 1.0$  and three different injection velocities  $v_{p0} = 0, 40$  and  $80 \text{ m/s}$

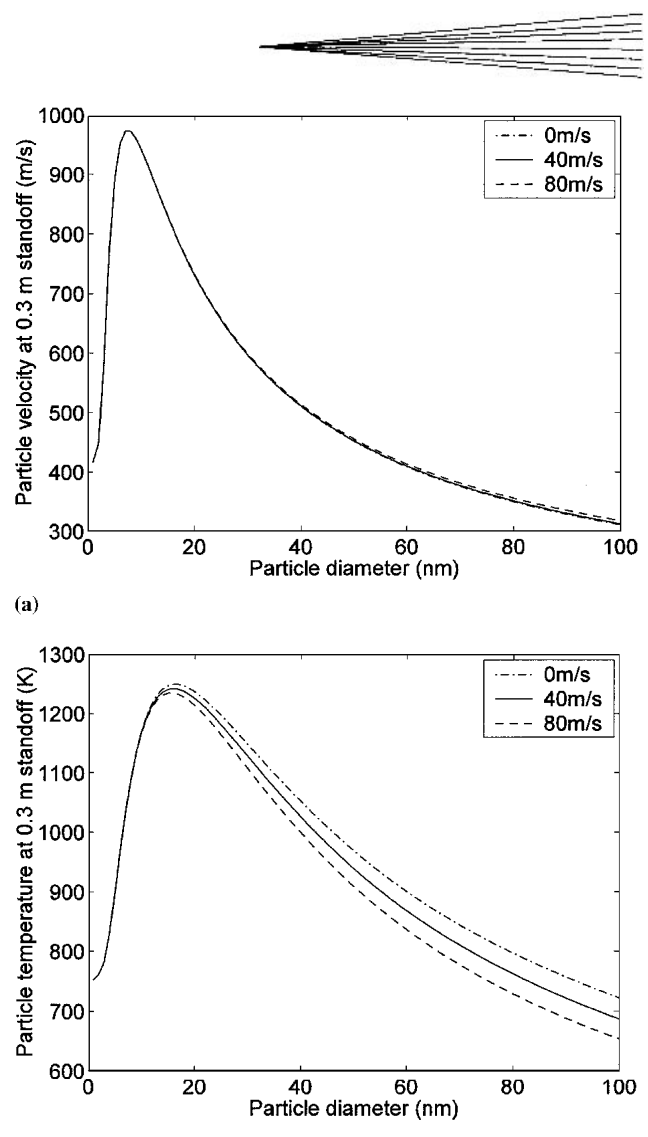
for the initial part), especially for particles with small sizes. This phenomena can be explained by Fig. 3(a), from which it can be seen that particles with larger injection velocity have a shorter acceleration stage and reach the critical point (where the gas and particle velocities are equal) sooner. Near the critical point, the drag force is very small. Second, larger particle injection velocity shortens the residence time of particles in the gas flame (refer to Fig. 3b), and as a consequence, particle temperature drops. Third, the disturbances on particle injection velocity have a more significant effect on particle temperature profile for coarse particles than finer ones. Note that the change of particle injection velocity has an effect on the process somewhat similar to changes in the injection position; the changes in the particle velocity and temperature at the point of impact on substrate are consistent with the experimental observations in Ref. 25.

Figure 4 shows the influence of combustion chamber pressure and equivalence ratio on the velocity and temperature pro-



**Fig. 4** Particle velocity and temperature as a function of (a) combustion chamber pressure  $p = 4, 7$ , and  $11$  bar,  $\varphi = 1.0$  and (b) equivalence ratio  $\varphi = 0.8, 1.0$ , and  $1.2$ ,  $p = 9$  bar)

files of an individual particle of size  $d_p = 40 \mu\text{m}$ . In Fig. 4(a), the equivalence ratio is fixed at 1.0 and the pressure in the combustion chamber varies from 4-11 bar. It can be seen that the particle velocity changes much more than the particle temperature. Furthermore, chamber pressure does not significantly influence gas velocity, while it affects particle velocity because the drag force on particle depends strongly on gas density, which, in turn, depends on chamber pressure (see also Ref. 16 for similar conclusions). In Fig. 4(b), the combustion chamber pressure is fixed at 9 bar and the equivalence ratio varies from 0.8-1.2. It is found that while the particle temperature changes significantly, the particle velocity remains almost constant. Particle temperatures are higher at 1.0 than those at  $\varphi = 1.2$  and  $\varphi = 0.8$ , which implies that when the reaction occurs close to stoichiometric condition it tends to achieve higher particle temperature. From these two figures, it can be concluded that the particle velocity is primarily influenced by the combustion chamber pressure and the particle temperature depends mainly on the equivalence ratio; a conclusion which is in good agreement with available experimental observations.<sup>[25, 26]</sup>



**Fig. 5** (a) Axial particle velocity and (b) temperature at the point of impact on substrate as a function of particle size and particle injection velocity. Operating conditions  $p = 9$  bar,  $\varphi = 1.0$

Figure 5 shows the particle velocity and temperature at the 0.3 m standoff under operating conditions  $p = 9$  bar,  $\varphi = 1.0$  in the particle size range 1-100  $\mu\text{m}$ . As particle diameter increases, both particle velocity and particle temperature increase first, and then decrease. The maximum values of both particle velocity and temperature corresponding to particle sizes between 15-25  $\mu\text{m}$  can be explained by the interplay of gas dynamics and particle mass/thermal inertia. It is well known that the particles are typically accelerated in the barrel and in some region of the free jet, and then they are decelerated. Particles of very small size have small mass inertias and are easily accelerated when the gas velocity is larger than the particle velocity. However, small particles are also easily decelerated when the particle velocity is larger than the gas velocity. On the other hand, large size particles are difficult to be accelerated as well as decelerated. As a result, particles with size between 15-25  $\mu\text{m}$  tend to have higher velocities at the point of impact on substrate than both bigger and smaller particles. A similar explanation can be given for the dependence of particle temperature at the point of impact on substrate on particle size.

## 2.5 Modeling of Powder Size Distribution

The fact that particle temperature and velocity at the point of impact on substrate depend strongly on particle size implies that particle size of the feedstock is one of the key parameters deciding coating quality. This property, together with the significant polydispersity of most powders used in the thermal spray process, motivates accounting for the effect of powder size distribution in the process model, the control problem formulation and the controller design. Previous experimental work (e.g., Ref. 27 and 28) has shown that lognormal functions can adequately describe the size distribution of many powders used in the HVOF process. To this end, a lognormal function is used in this paper to describe the powder size distribution with the following form<sup>[29]</sup>:

$$f(d_p) = \frac{1}{\sqrt{2\pi}\sigma d_p} \exp\left[-\frac{(\ln d_p - \mu)^2}{2\sigma^2}\right], \quad (\text{Eq 12})$$

where  $f(d_p)$  is the size distribution function,  $\mu$  and  $\sigma^2$  are two dimensionless parameters corresponding to the mean and the variance of  $\ln d_p$ , which obeys the normal distribution. For particles that are lognormally distributed,  $\mu$  and  $\sigma$  can be determined using the following formulae<sup>[30]</sup>:

$$\mu = \ln^3 \sqrt{d_{10} d_{50} d_{90}} - 1.831 \left( \ln \sqrt{\frac{d_{90}}{d_{10}}} \right)^2 \quad (\text{Eq 13})$$

$$\sigma = 0.781 \ln \sqrt{\frac{d_{90}}{d_{10}}},$$

where  $d_{10}$ ,  $d_{50}$ , and  $d_{90}$  are three characteristic diameters, which can be obtained experimentally.<sup>[11]</sup>

There are many ways to define average powder properties. For example, they can be averaged with respect to particle number or particle volume. In this work, the average powder properties ( $PP$ ) are calculated based on particle volume because larger particles have a stronger influence on coating properties than smaller ones. Volume-based average powder properties can be computed as follows:

$$\overline{PP} = \frac{\int_0^\infty \frac{1}{6} \pi d_p^3 PP(d_p) f(d_p) d(d_p)}{\int_0^\infty \frac{1}{6} \pi d_p^3 f(d_p) d(d_p)}. \quad (\text{Eq 14})$$

## 3. Feedback Control of HVOF Thermal Spray Process

### 3.1 Control Problem Formulation and Controller Design

Based on the model predictions, and the available experimental results, the control problem for the HVOF system is formulated as one of regulating the volume-based averages of temperature and velocity of particles at impact on the substrate (these are the variables that directly influence coating microstructure and porosity) by manipulating the combustion chamber pressure and the oxygen/fuel ratio. From the simulation results of subsection 2.4, it follows that  $\rho_{\text{g}}$ , which strongly affects

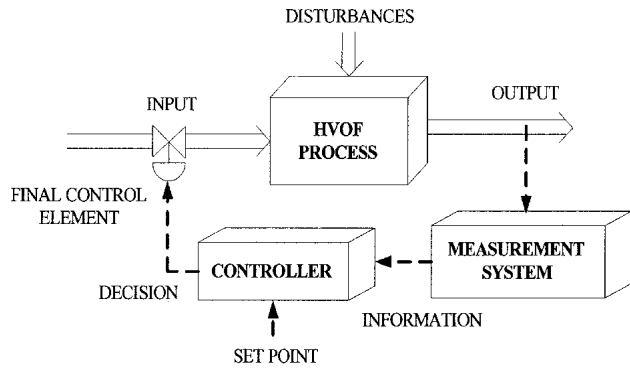


Fig. 6 Schematic of the HVOF control system

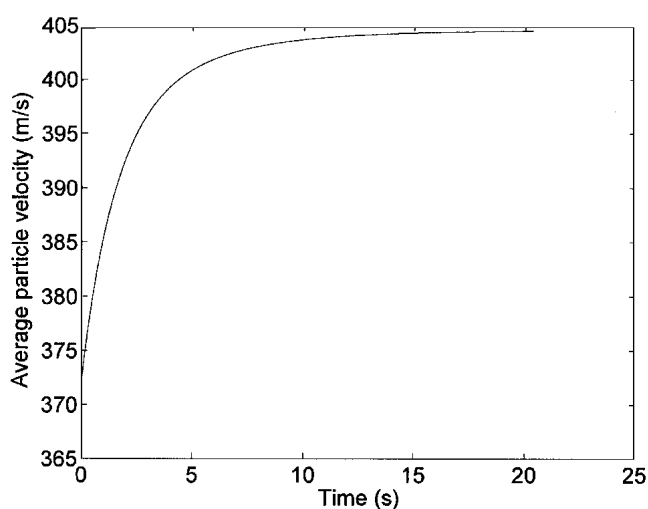
$v_p$ , and  $T_g$ , which strongly affects  $T_p$ , can be almost independently adjusted by manipulating the combustion chamber pressure,  $u_1(t)$ , which is related to total gas flow rate, and the equivalence ratio,  $u_2(t)$ , respectively. At this point, it is important to note that control of an average particle property, such as volume-averaged particle temperature and velocity, is all that can be achieved using two lumped manipulated variables. Control of velocity and temperature of individual particles or of particles with different sizes cannot be achieved with just two manipulated variables. The usefulness of the proposed approach based on volume-averaged particle velocity and temperature will be shown in the next subsection.

The proposed formulation of the control problem can be readily used in the context of experimental HVOF systems because both the chamber pressure and the equivalence ratio can be manipulated in real-time, by adjusting the total flow rate of fuel and oxidant (Eq 7) and their ratio, respectively. A schematic of the feedback control system for the HVOF process is shown in Fig. 6. The manipulated input variables are the flow rates of oxygen and fuel; these are the variables that can be adjusted by the control system to change the behavior of the process. The controlled output variables, which are the variables that the controller tries to set at desired values, are the average particle velocity and temperature before impact on the substrate, which can be measured experimentally using non-intrusive optical techniques, for example, laser Doppler velocimetry,<sup>[30]</sup> particle imaging velocimetry,<sup>[31, 32]</sup> and two color pyrometry,<sup>[14, 25, 33]</sup> etc. The controller obtains information from the measurement system and makes decisions, which are sent to the controlled valves (total flow of gases to the process and oxygen/fuel ratio), to adjust the manipulated input variables until the deviation of the controlled outputs from their corresponding set-point values falls within a tolerable region. One of the great advantages of feedback control is that it can compensate for the effect of disturbances in the process operating conditions.

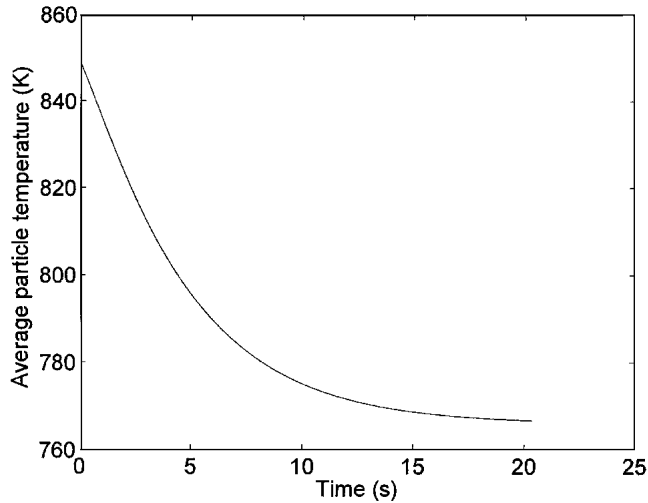
Because the almost decoupled nature of the manipulated input/controlled output pairs, two proportional integral (PI) controllers are used to regulate the process. Specially, the controllers have the following form:

$$\zeta_i = y_{\text{sp}_i} - y_i, \quad \zeta_i(0) = 0, \quad i = 1, 2$$

$$u_i = K_{c_i} (y_{\text{sp}_i} - y_i) + \frac{1}{\tau_{c_i}} \zeta_i + u_{0_i}, \quad i = 1, 2 \quad (\text{Eq 15})$$



(a)



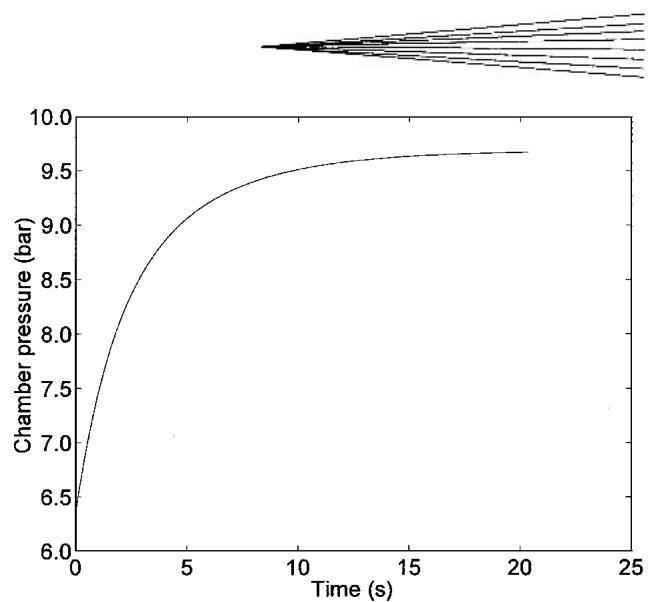
(b)

**Fig. 7** Profiles of volume-based average (a) particle velocity and (b) particle temperature with respect to time; control problem formulation accounting for powder size distribution

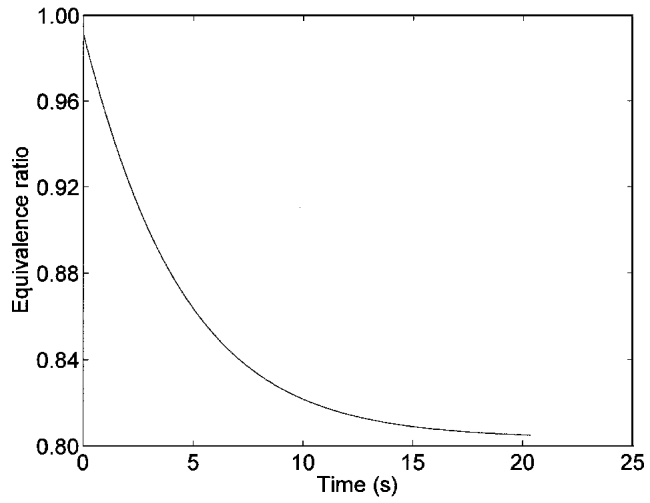
**Table 2** Process Parameters Used in the Closed-Loop Simulation

Parameters	Values
$K_{c1}$	$1 \times 10^3$
$K_{c2}$	$1 \times 10^{-3}$
$\tau_{c1}$	0.2
$\tau_{c2}$	0.2
$d_{10}$	27 $\mu\text{m}$
$d_{50}$	80 $\mu\text{m}$
$d_{90}$	144 $\mu\text{m}$
$\psi$	1.0

where  $y_{sp_i}$  is the desired set-point value,  $y_i$  is the value of the output obtained from the measurement system ( $y_1$  is average particle velocity and  $y_2$  is average particle temperature),  $u_i$  is the manipulated input ( $u_1$  is the chamber pressure and  $u_2$  is the



(a)



(b)

**Fig. 8** Profiles of (a) chamber pressure and (b) equivalence ratio with respect to time; control problem formulation accounting for powder size distribution

equivalence ratio).  $K_{c_i}$  is the proportional gain and  $\tau_{c_i}$  is the integral time constant. The values of the controller parameters  $K_{c_i}$  and  $\tau_{c_i}$  were chosen to achieve smooth controlled output transient responses in the closed-loop system (i.e., process model under feedback control) without using unrealistically large control action (see simulation results in the next subsection). From Eq 15 it is easy to see that the controller includes integral action, which means that  $u_i$  will continuously change with time until the deviation of the measured output from its set point value is zero. Finally, note that while the shape of the powder size distribution is accounted for in the formulation of the control problem (i.e., selection of controlled outputs  $y_1$  and  $y_2$ ), the feedback control system of Eq 15 does not make direct use of the process model. The design of a model-based feedback control system, employing nonlinear control techniques for particulate processes (see Ref. 34, 35, 36, 38, and 39] for details), as well as applications of the control system to more detailed HVOF process model (i.e.,

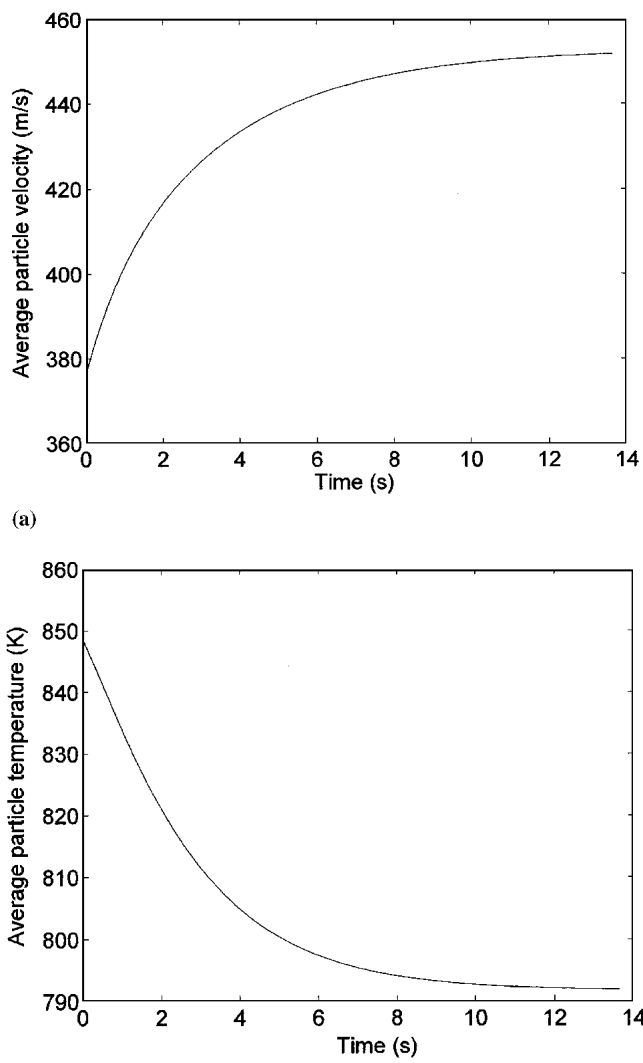


**Fig. 9** Profiles of (a) volume-based average particle velocity and (b) particle temperature with respect to time; control problem formulation without accounting for powder size distribution

two-dimensional in space models for gas and particle motion and temperature) and an experimental system, will be the subject of future work.

### 3.2 Simulation Results of HVOF Process Model Under Feedback Control

In this subsection, simulation runs of the closed-loop system are presented. In several cases, the outputs of the closed-loop system are compared with the outputs of the open-loop system (i.e., process model with  $P$  and  $\varphi$  set at fixed values). The outputs  $y_1(t)$  and  $y_2(t)$  are computed by averaging the individual particle velocity and temperature data obtained from the process model using Eq 14. To account for the powder size distribution, up to 100 particles of different size are traced simultaneously to obtain the average velocity and temperature. This requires solving simultaneously 300 ordinary differential equations. The parameters used in the closed-loop system simulations are shown in Table 2.

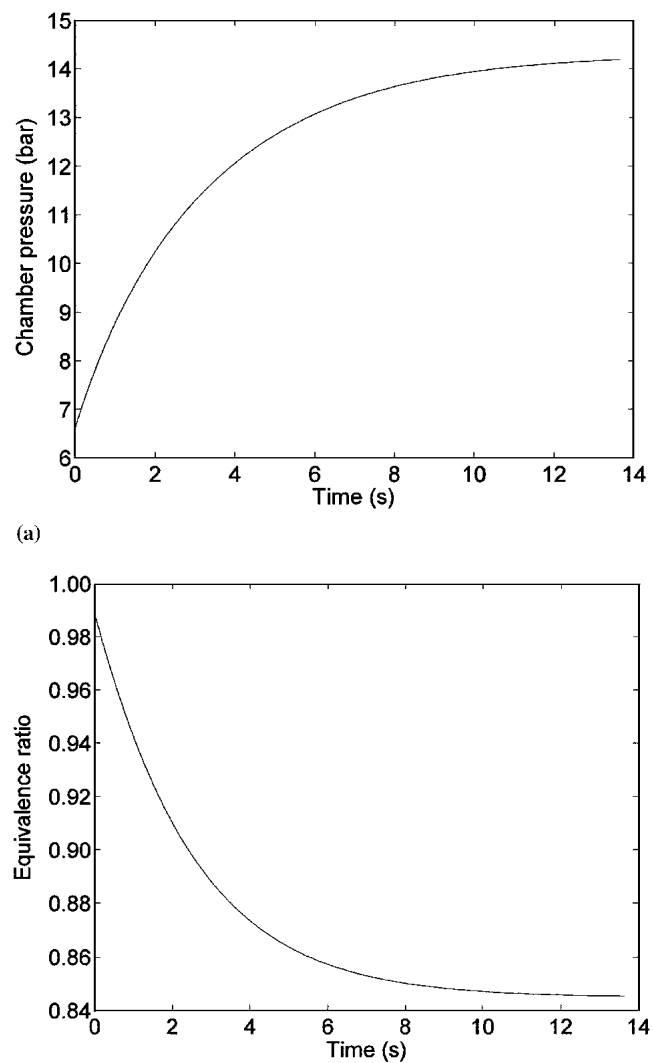
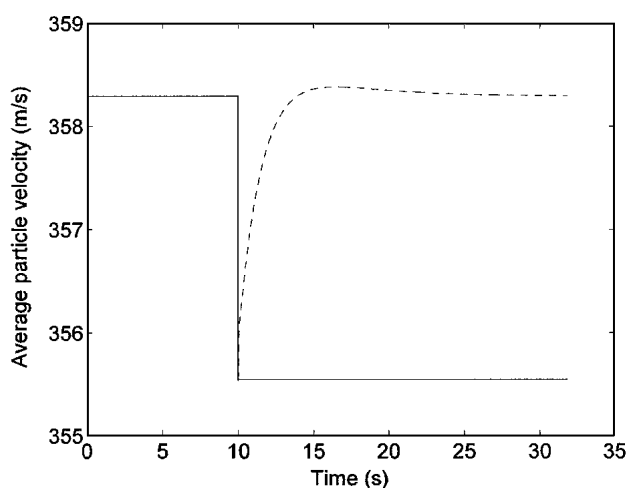
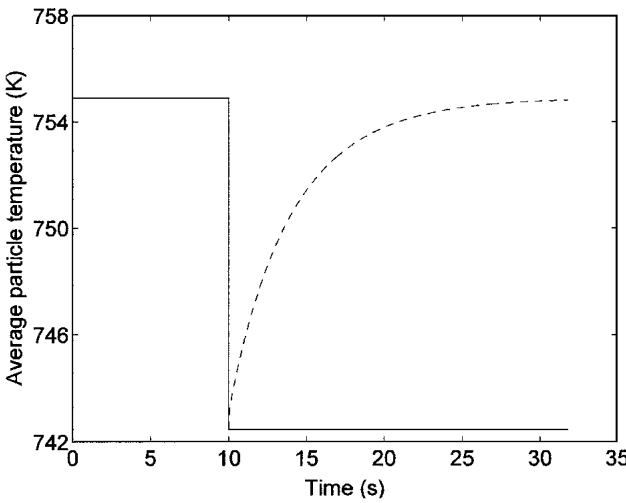


**Fig. 10** Profiles of (a) chamber pressure and (b) equivalence ratio with respect to time; control problem formulation without accounting for powder size distribution

Several simulation runs of the process model under the feedback controller were performed to evaluate the ability of the controller: (1) to drive the particle temperature and velocity at the point of impact on substrate to desired set-point values, and (2) to attenuate the effect of disturbances on process operating conditions. In addition, the proposed formulation and solution to the control problem is compared with an approach, which assumes monodisperse powder size distribution. The first simulation studies the behavior of the closed-loop system in the presence of changes in the set-point. Initially, the process is assumed to operate at  $p = 6$  bar and  $\varphi = 1.0$  (which corresponds to  $v_p = 367.8$  m/s and  $T_p = 851.1$  K), and at time  $t = 0$  s, the average particle velocity set-point value increases by 10% and the average particle temperature set-point value decreases by 10%. Figure 7 and 8 show how the controlled outputs ( $v_p$  and  $T_p$ ) and manipu-



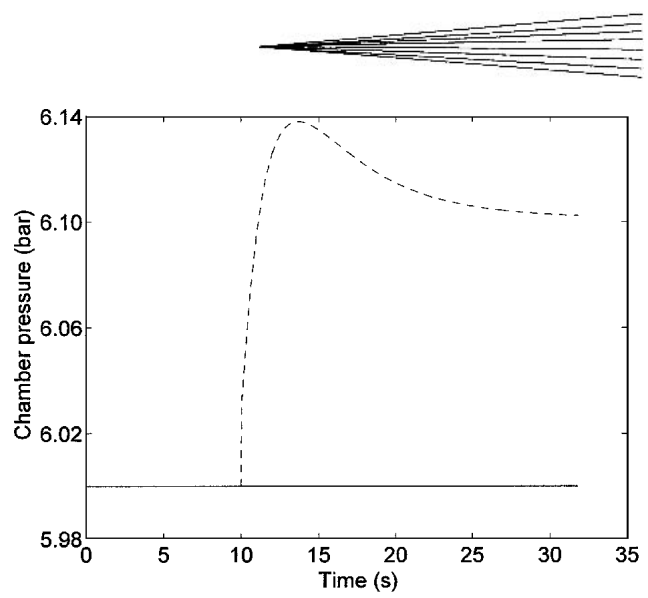
(a)



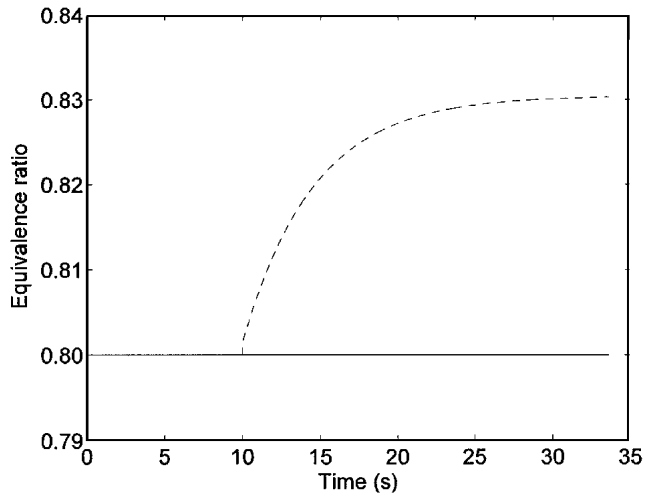
(b)

**Fig. 11** Profiles of (a) volume-based average particle velocity and (b) particle temperature with respect to time in the presence of a 30% disturbance on spray distance; open-loop system (solid curve) and closed-loop system (dashed curve)

lated inputs ( $P$  and  $\varphi$ ) move in the case of requesting such changes in the set-point values. The feedback controller drives the controlled outputs to the new set points ( $v_p = 404.6$  m/s and  $T_p = 766.7$  K) in about 20 s (note that 20 s is the time needed for the controlled outputs to reach the new set-point values, not the time for the particles to hit the substrate, which is on the order of  $10^{-3}$  s). Further investigation of Fig. 7 shows that the time needed to achieve 90% of the desired set-point values is about 5 s for particle velocity and 10 s for particle temperature, which means that the controller is quite effective and validates the feasibility of implementation of feedback control on the HVOF process. We also note that faster closed-loop output response can be achieved at the expense of using larger control action (i.e., larger values for  $\varphi$  and  $P$ ); in practice, the speed of the closed-loop response (and thus, the optimal values of  $K_{c_i}$  and  $\tau_{c_i}$ ) depends on the specific HVOF thermal spray system and should be determined using several experiments.



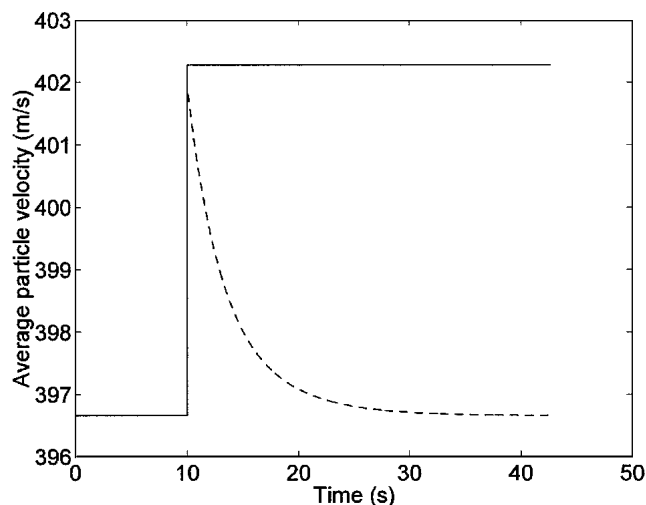
(a)



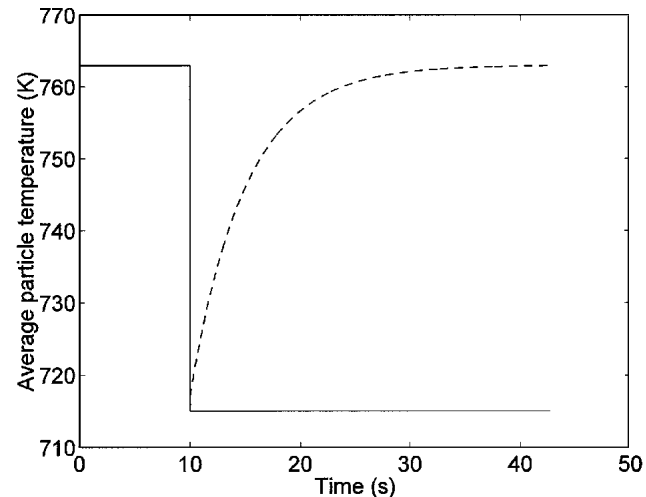
(b)

**Fig. 12** Profiles of (a) chamber pressure and (b) equivalence ratio with respect to time in the presence of a 30% disturbance on spray distance; open-loop system (solid curve) and closed-loop system (dashed curve)

To show that the proposed formulation of the control problem (which explicitly accounts for the effect of powder size distribution) leads to a solution of the control problem that is superior (with respect to the control action needed to achieve the desired control objectives) to a solution that assumes a mono-disperse powder size distribution, the two PI controllers are also implemented on the process model using the same controlled outputs but assuming that the velocity and temperature measurements are based on a single particle whose size is taken to be  $d_p = 20$   $\mu\text{m}$ . The corresponding controlled and manipulated variables are given in Fig. 9 and 10, respectively. The results show that the average particle velocity increases by 22.9% (final  $v_p = 451.8$  m/s) and the average particle temperature decreases by 7.0% (final  $T_p = 791.9$  K). Therefore, the desired objectives of 10% change in the set-point values are not achieved (compare the controlled output profiles of Fig. 9 and 7, where the desired set-point change is achieved); this occurs because, as it has been



(a)

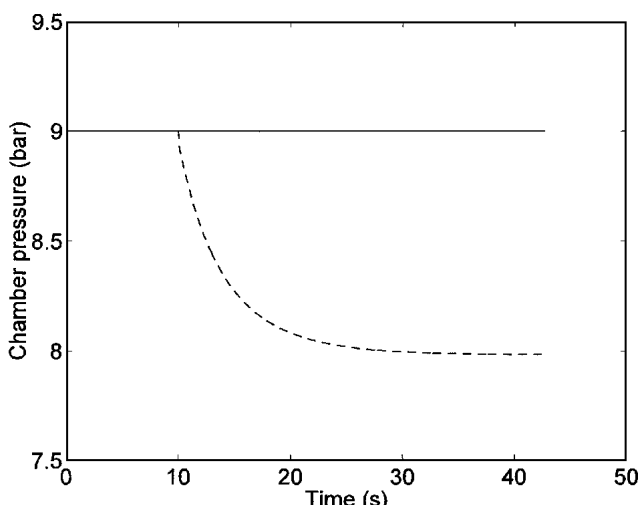


(b)

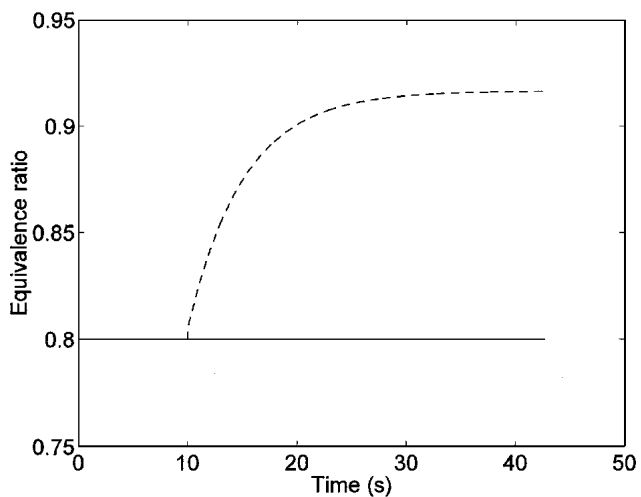
**Fig. 13** Profiles of (a) volume-based average particle velocity and (b) particle temperature with respect to time in the presence of 80 m/s variation in initial particle velocity; open-loop system (solid curve) and closed-loop system (dashed curve)

previously shown, the behavior of an individual particle is insufficient to represent that of the entire powder size distribution. This makes clear the need to account for the effect of powder size distribution in the control problem formulation and solution.

To test the robustness of the proposed control problem formulation and of the feedback controller, the problem of controlling the HVOF process in the presence of disturbances was studied. Figure 11 and 12 show the controlled output and manipulated input profiles in the presence of 30% disturbance in the spray distance (i.e., the spray distance increases from 0.3 m to 0.39 m and then stays at this value) which occurs at  $t = 10$  s. Without control, the process jumps to a new steady state in a very short time (owing to the very short time of particle flight), and both the particle velocity (solid curve in Fig. 11a) and temperature (solid curve in Fig. 11b) drop instantaneously due to further particle cooling and deceleration. With feedback control,



(a)

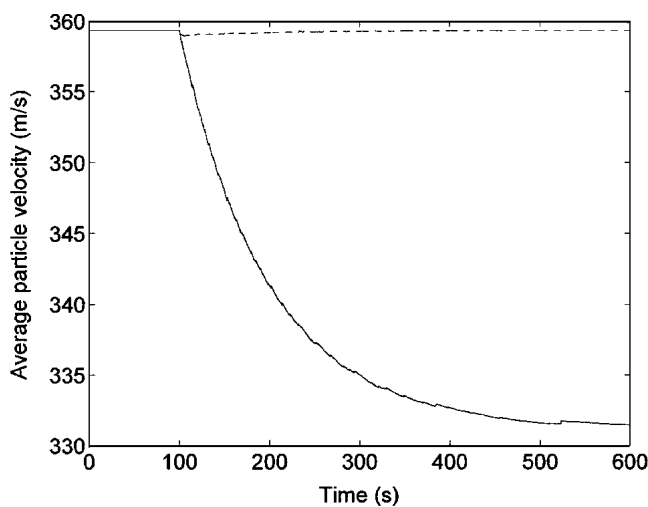


(b)

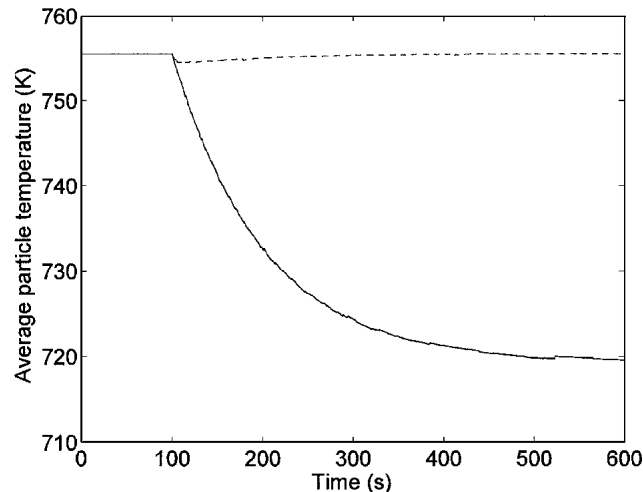
**Fig. 14** Profiles of (a) chamber pressure and (b) equivalence ratio with respect to time in the presence of 80 m/s variation in initial particle velocity. Open-loop system (solid curve) and closed-loop system (dashed curve).

the process outputs (dashed curves in Fig. 11a and 11b) move gradually and finally achieve their desired set-point values in about 30 s.

Figure 13 and 14 show the controlled output and manipulated input profiles in the presence of 80 m/s change in initial particle velocity at  $t = 10$  s. Without control, the system jumps to a new steady state in a very short time. The impact particle velocity increases by about 6 m/s while the impact particle temperature decreases by about 48 K. The drop of particle temperature is explained by the shortened residence time of particles in the flame gas, which is caused by an increase of the particle velocity along the flight, although the particle velocity at the point of impact remains nearly the same. Such a temperature change can have a significant effect on the molten state of the particle and the resulting coating microstructure. Under feedback control, the manipulated inputs drive the pro-



(a)



(b)

**Fig. 15** Profiles of (a) volume-based average particle velocity and (b) particle temperature with respect to time in the presence variation in powder size distribution; open-loop system (solid curve) and closed-loop system (dashed curve)

cess outputs to their original steady state values in about 30 s, attenuating the effect of disturbance on particle injection velocity.

Another source of disturbance, especially in an industrial environment, is the variation of the size distribution of the powder during the operation of the HVOF process. This may have a significant influence on the particle velocity and particle temperature at the point of impact on the substrate based on the analysis of the previous sections. In the following simulation, it is assumed that the process is at steady state in the first 100 s and then the powder size distribution changes gradually (specifically, in the following calculation,  $\mu$  increases according to the expression  $\mu = \mu_0[1 + 0.05(1 - \exp(-t/100))]$  and  $\sigma^2$  is kept constant). To reduce the computational cost of this closed-loop simulation, the integral time step for the particle motion and temperature equation is taken to be  $5 \times 10^{-6}$  s instead of  $10^{-7}$  s, and the total number of particles with different sizes, which are simultaneously traced, is taken to be 40 instead of 100. Figure 15 and 16

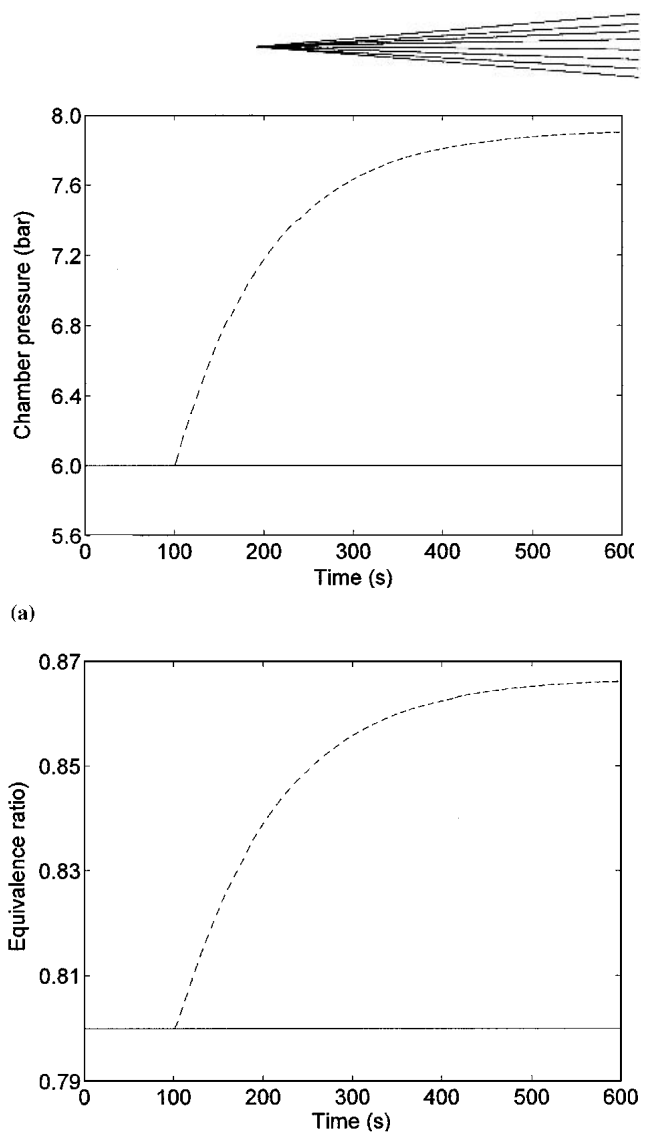


**Fig. 16** Profiles of (a) chamber pressure and (b) equivalence ratio with respect to time in the presence of variation in powder size distribution; open-loop system (solid curve) and closed-loop system (dashed curve)

(dashed curves) show the controlled outputs and the manipulated inputs in the presence of such a variation in the powder size distribution. Both particle velocity (Fig. 15a) and temperature (Fig. 15b) fluctuate in a very narrow range and eventually reach the desired set-point values. When no control is used (Fig. 15 and 16 solid curves), in which case the chamber pressure and the equivalence ratio are kept constant, both particle velocity and particle temperature decrease with time, which may have an undesirable effect on the resulting coating properties. In summary, the closed-loop system simulations in the presence of disturbances show that the controller attenuates the effect of disturbances and drives the controlled outputs to the desired set-point values within about 20 s. Faster disturbance rejection could be achieved at the expense of using larger control action; for an experimental HVOF system, the optimal speed of disturbance rejection should be determined on the basis of the system response to the disturbances.

## 4. Conclusion

This work presented a formulation of the control problem and a feedback control system for the HVOF thermal spray process, which explicitly account for the effect of powder size distribution. Specifically, the control problem was formulated as the one of regulating volume-based averages of the temperature and velocity of the particles at the point of impact on substrate by manipulating the oxygen/fuel ratio and the combustion chamber pressure, respectively. Simulation runs of the process model under the feedback controller showed that the proposed approach to control leads to effective regulation of the particle velocity and temperature at the point of impact on substrate and is robust with respect to significant variations in the process operating conditions and powder size distribution.

## Acknowledgments

Financial support from a 2001 Office of Naval Research Young Investigator Award, program manager Dr. Lawrence Kabaoff, is gratefully acknowledged. The authors would also like to thank the anonymous reviewers for their comments and suggestions.

## References

1. M.L. Lau, H.G. Jiang, W. Nuchter, and E.J. Lavernia: "Thermal spraying of nanocrystalline Ni coatings," *Phys. Status Solidi A*, 1998, **166**, pp. 257-68.
2. D. Cheng, G. Trapaga, J.W. McKeliget, and E.J. Lavernia: "Mathematical Modeling of High Velocity Oxygen Fuel Thermal Spraying: An Overview," *Key Eng. Mater.*, 2001, **197**, pp. 1-25.
3. V.L. Tellkamp, M.L. Lau, A. Fabel, and E.J. Lavernia: "Thermal Spraying of Nanocrystalline Inconel 718," *Nanostruct. Mater.*, 1997, **9(1-8)**, pp. 489-92.
4. G.D. Power, T.J. Barber, and L.M. Chiappetta: "Analysis of a High Velocity Oxygen-fuel (HVOF) Thermal Torch" in *28th AIAA/SAE/ASME/ASEE Joint Propulsion Conference and Exhibit*, AIAA92-3598, Nashville, Tennessee, 1992.
5. X. Yang and S. Eidelman: "Numerical Analysis of a High-Velocity Oxygen-fuel Thermal Spray System," *J. Therm. Spray Technol.*, 1996, **5(2)**, pp. 175-84.
6. B. Hassan, A.R. Lopez, and W.L. Oberkampf: "Computational Analysis of a Three-Dimensional High-Velocity Oxygen Fuel (HVOF) Thermal Spray Torch," *J. Therm. Spray Technol.*, 1998, **7(1)**, pp. 71-77.
7. G.-X. Wang, V. Prasad, and S. Sampath: "Rapid Solidification in Thermal Spray Deposition: Microstructure and Modelling" in *Sadhana*, 2001, **26**, pp. 35-57.
8. V. Gourlaouen, E. Verna, and P. Beaubien: "Influence of Flame Parameters on Stainless Steel Coatings Properties" in *Thermal Spray: Surface Engineering via Applied Research, Proceedings of the International Thermal Spray Conference*, C.C. Berndt and S. Sampath, ed., ASM International, Materials Park, OH, 2000, Montreal, QC, Canada, pp. 487-93.
9. A.V. Zagorski and F. Stadelmaier: "Full-scale Modelling of a Thermal Spray Process," *Surf. Coat. Technol.*, 2001, **146-147**, pp. 162-67.
10. S. Annavarapu, D. Apelian, and A. Lawley: "Spray Casting of Steel Strip: Process Analysis," *Metall. Trans. A*, 1990, **21**, pp. 3237-56.
11. P. Marthur, S. Annavarapu, D. Apelian, and A. Lawley: "Spray Casting: An Integral Model for Process Understanding and Control," *Mater. Sci. Eng. A*, 1991, **142**, pp. 261-76.
12. J.R. Fincke, W.D. Swank, R.L. Bewley, D.C. Haggard, M. Gevelbar, and D. Wroblewski: "Diagnostics and Control in the Thermal Spray Process," *Surf. Coat. Technol.*, 2001, **146-147**, pp. 537-43.
13. C. Moreau and L. Leblanc: "Optimization and Process Control for High Performance Thermal Spray Coatings," *Key Eng. Mater.*, 2001, **197**, pp. 27-57.
14. W.D. Swank, J.R. Fincke, and D.C. Haggard: "A Particle Temperature Sensor for Monitoring and Control of the Thermal Spray Process" in *Proc. 8th Natl. Thermal Spray Conf.*, C.C. Berndt and S. Sampath, ed., ASM International, Materials Park, OH 1995, pp. 111-16.
15. J.A. Roberson and C.T. Crowe: *Engineering Fluid Dynamics*, John Wiley & Sons, New York, 1997.
16. W.D. Swank, J.R. Fincke, D.C. Haggard, and G. Irons: "HVOF Gas Flow Field Characteristics" in *Proc. 7th Natl. Thermal Spray Conf.*, C.C. Berndt and S. Sampath, ed., ASM International, Materials Park, OH 1994, pp. 313-18.
17. S. Gordon and B.J. McBride: "Computer Program for Calculation of Complex Chemical Equilibrium Compositions and Applications," NASA Reference Publication 1311, Lewis Research Center, Cleveland, OH, 1994.
18. H.H. Tawfik and F. Zimmerman: "Mathematical Modeling of the Gas and Powder Flow in HVOF Systems," *J. Therm. Spray Technol.*, 1997, **6(3)**, pp. 345-52.
19. L. Pawlowski: *The Science and Engineering of Thermal Spray Coatings*, John Wiley & Sons, Chichester, UK, 1995.
20. D. Cheng, Q. Xu, G. Trapaga, and E.J. Lavernia: "The Effect of Particle Size and Morphology on the In-flight Behavior of Particles During High-Velocity Oxyfuel Thermal Spraying," *Metall. Mater. Trans. B*, 2001, **32(3)**, pp. 525-35.
21. G.H. Ganser: "A Rational Approach to Drag Prediction of Spherical and Nonspherical Particles," *Powder Technol.*, 1993, **77**, pp. 143-52.
22. C.J. Geankolis, *Transport Processes and Unit Operations*, Prentice-Hall, NJ, 1993.
23. R.B. Bird, W.E. Stewart, and E.N. Lightfoot: *Transport Phenomena*, John Wiley & Sons, New York, 1960.
24. C.T. Crowe and D.E. Stock: "A Computer Solution for Two-dimensional Fluid-particle Flows," *Int. J. Numerical Meth. Eng.*, 1976, **10**, pp. 185-96.
25. T.C. Hanson, C.M. Hackett, and G.S. Settles: "Independent Control of HVOF Particle Velocity and Temperature," *J. Therm. Spray Technol.*, 2002, **11(1)**, pp. 75-85.
26. W.D. Swank, J.R. Fincke, D.C. Haggard, and G. Irons: "HVOF Particle Flow Field Characteristics" in *Proc. 7th Natl. Thermal Spray Conf.*, C.C. Berndt and S. Sampath, ed., ASM International, Materials Park, OH, 1994, pp. 319-24.
27. R. Lima, A. Kucuk, and C.C. Berndt: "Integrity of Nanostructured Partially Stabilized Zirconia after Plasma Spray Processing," *Mater. Sci. Eng. A*, 2001, **313**, pp. 75-82.
28. E.J. Lavernia and Y. Wu: *Spray Atomization and Deposition*, John Wiley & Sons, Chichester, England, 1996.
29. E.L. Crow and K. Shimizu, *Lognormal Distributions: Theory and Applications*, Marcel Dekker, New York, 1988.
30. M. Li and P.D. Christofides: "Modeling and Analysis of HVOF Thermal Spray Process Accounting for Powder Size Distribution," *Chem. Eng. Sci.*, 2003, **58**, pp. 849-57.
31. J.R. Fincke, W.D. Swank, and C.L. Jeffrey: "Simultaneous Measurement of Particle Size, Velocity and Temperature in Thermal Plasmas," *IEEE Trans. Plasma Sci.*, 1990, **18(6)**, pp. 948-57.
32. R. Knight, R.W. Smith, and Z. Xiao: "Particle Velocity Measurements in HVOF and APS Systems" in *Proc. 7th Natl. Thermal Spray Conf.*, C.C. Berndt and S. Sampath, ed., ASM International, Materials Park, OH, 1994, pp. 331-36.
33. I. Thomson, V. Pershin, J. Mostaghimi, and S. Chandra: "Experimental Testing of a Curvilinear Gas Shroud Nozzle for Improved Plasma Spraying," *Plasma Chem. Plasma Proc.*, 2001, **21(1)**, pp. 65-82.
34. J.R. Fincke, D.C. Haggard, and W.D. Swank: "Particle Temperature Measurement in the Thermal Spray Process," *J. Therm. Spray Technol.*, 2001, **10**, pp. 255-66.
35. T. Chiu and P.D. Christofides: "Nonlinear Control of Particulate Processes," *AIChE J.*, 1999, **45**, pp. 1279-97.
36. A. Kalani and P.D. Christofides: "Nonlinear Control of Spatially-Inhomogeneous Aerosol Processes," *Chem. Eng. Sci.*, 1999, **54**, pp. 2669-78.
37. P.D. Christofides: *Model-Based Control of Particulate Processes*, Particle Technology Series, Kluwer Academic Publishers, The Netherlands, 2002.
38. T. Chiu and P.D. Christofides: "Robust Control of Particulate Processes Using Uncertain Population Balances," *AIChE J.*, 2000, **46**, pp. 266-80.
39. N.H. El-Farra, T. Chiu, and P.D. Christofides: "Analysis and Control of Particulate Processes With Input Constraints," *AIChE J.*, 2001, **47**, pp. 1849-65.